Controlling the Wettability of Plastic by Thermally Embedding Coated Aluminium Oxide Nanoparticles into the Surface

Donald Hill,[a] *Andrew R. Barron,*[a,b,c] *and Shirin Alexander*[*a]

[a]*Energy Safety Research Institute (ESRI), Swansea University Bay Campus, Fabian Way, Swansea SA1 8EN, United Kingdom.*

[b]*Department of Chemistry, Rice University, Houston, Texas 77005, USA.*

[c]*Department of Materials Science and Nanoengineering, Rice University, Houston, TX 77005, USA.*

*Corresponding Author. E-mail: s.alexander@swansea.ac.uk

Keywords: *superhydrophobic surfaces, nanoparticles, durable, branched carboxylic acid, Al_2O_3, thermal embedding.*

Abstract

Hypothesis

Nanoparticle embedding into the surface of plastics provides an effective anchor that improves the durability of coatings formed from functionalized nanoparticles. Coatings formed from thermally embedded particles show superior wear resistance relative to coatings formed from non-embedded particles. As a consequence of this, embedded nanoparticles functionalized with hydrophilic and hydrophobic carboxylates are better suited for controlling the wettability of plastics than when the nanoparticles are deposited onto the plastic under ambient conditions.

Experiments

Carboxylate-functionalized Al_2O_3 nanoparticles were embedded into ethylene vinyl acetate through spray coating the particles onto the substrate during heating. Sonication was used to remove excess particles that did not become embedded into the material. Coatings formed from the embedded particles were characterized through scanning electron microscopy (SEM), atomic force microscopy (AFM), energy dispersive x-ray spectroscopy (EDX), and x-ray photoelectron spectroscopy (XPS). The wettability of the coatings was characterized using static and dynamic contact angle (CA) measurements to measure the apparent water contact angles, and sliding angle measurements, whilst the durability of the coatings was studied using scratch testing, tape peel tests, and abrasion tests. The build-up of fog on the substrates was also studied through exposing the surfaces to water vapour.

Findings

Thermal embedding of the particles into the surface of the plastic was observed to occur when the material was heated to temperatures around its melting temperature. AFM and SEM showed that plastic embedded with the nanoparticles possessed a morphology that was substantially rougher than the untreated plastic. CA measurements showed that plastic embedded with hydrophobic isostearate functionalized nanoparticles was highly hydrophobic and displayed a CA of approximately 152º. Dynamic CA measurements and sliding angle measurements revealed that plastic embedded with the isostearate functionalized nanoparticles showed petal-like wetting behavior. Furthermore, it was observed that the CA of the plastic could be varied from highly hydrophobic to highly hydrophilic through embedding varying amounts of isostearate and hydrophilic 2-[2-(2-methoxyethoxy)ethoxy]acetate functionalised Al_2O_3 nanoparticles into the surface of the material. Scratch testing showed that thermally embedding the nanoparticles into the plastic substantially improved their abrasion resistance, relative to when the nanoparticles are deposited onto the non-heated material. This methodology indicates that embedding nanoparticles into plastics creates

durable coatings that can display variable wettability. Consequently, this methodology could be useful in applications where it is desirable to keep plastics dry, such as for food packaging or medical devices.

1. Introduction

Improving the durability of superhydrophobic coatings still remains a major challenge within the research community. Coatings created using functionalised nanoparticles have been studied due to their low wettability and ease at which they can be applied onto different surfaces.[1-6] However, despite their potential utility, these coatings show poor abrasion resistance, which limits their use in practical applications. To overcome this, composite coatings have been developed that improve the coatings' durability through embedding the nanoparticles in polymer films[7-9] and mixing them with resins.[10-13] These materials can either be pre-cast onto the substrate using techniques such as spin[9] or spray[10] coating or can be added directly to suspensions containing the nanoparticles.[11,13] For example, Si et al. prepared robust water-repellent surfaces using suspensions containing functionalised MgO and TiO_2 nanoparticles and epoxy resin.[11] These coatings showed remarkable durability when subjected to knife-scratch and sandpaper abrasion tests, and were resistant to some forms of chemical damage.[11]

Despite their effectiveness, these techniques increase the number of materials and steps required during the fabrication processes. Furthermore, the monomers that are used to produce commercially available adhesives like epoxy resin are often harmful to the population and environment,[14] and it is desirable to avoid their release if possible. As a consequence of these factors it is necessary to investigate other approaches that can improve the adhesion of nanoparticles onto substrates. Thermally embedding nanoparticles into surfaces has been reported for materials such as

glass,[15] graphene,[16] and plastics.[17-19] During this process the materials are heated to temperatures greater than or approaching their glass transition temperatures, which affects softening of the materials so that they are in liquid-like state. In this state particles on the surface can penetrate into the material and become embedded in the surface layers.[17] For example, Teichroeb and Forrest showed that it was possible to embed Au nanoparticles into polystyrene through heating the polymer to temperatures close to its bulk transition temperature.[19] AFM indicated that the nanoparticles were partially embedded into the polymer, with a large proportion of the total particle diameter protruding outside the material.[19]

Embedding nanoparticles into polymers has been used for a variety of purposes, such as to affect changes in the optical properties,[21,21] as a probe to study glass transition temperatures,[19,22] or in sensing applications.[24,25] However, to our knowledge, this methodology has not yet been used to control the wettability of surfaces. Furthermore, investigations into the durability of thermally embedded nanoparticles have not yet been undertaken. Herein, we investigate the embedding of isostearate and 2-2-2-methoxyethoxyethoxy acetate functionalised Al_2O_3 nanoparticles into plastic as route to control its apparent water contact angle (CA). Functionalisation is achieved through refluxing the particles with the desired carboxylic acid in toluene. Embedding the particles into the plastic was then carried out through spray coating and subsequent sonication (Scheme 1). Sonication was used to remove non-embedded particles from the plastic. The wear resistance of the plastic embedded with the isostearate functionalised Al_2O_3 nanoparticles, relative to the analogous non-heated nanoparticle coating is also reported in this study.

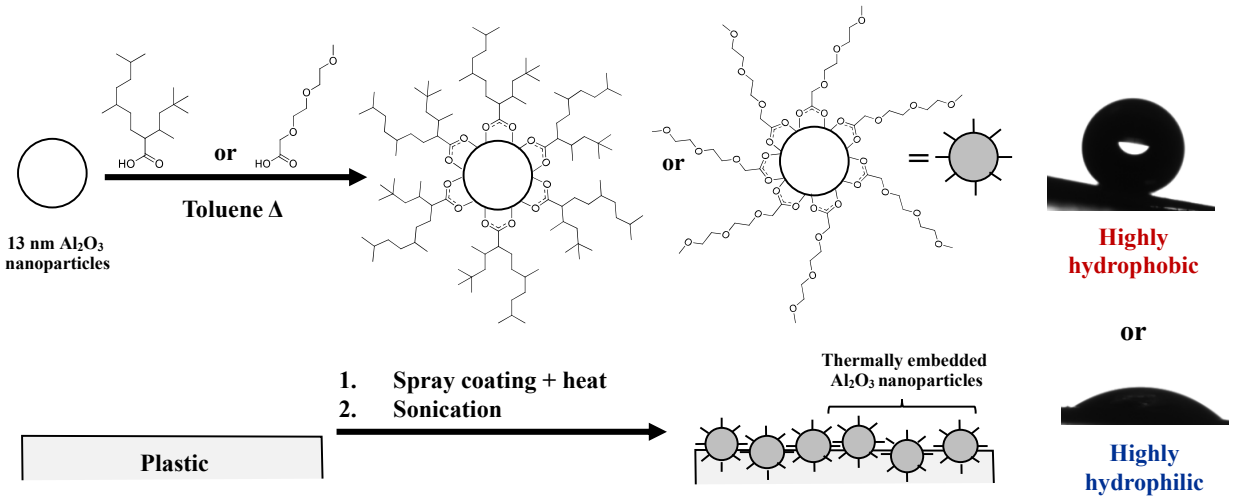

Scheme 1. Diagram showing the methods used to synthesise the nanoparticles and embed the particles into the plastic substrate.

2. Experimental methods

Materials and reagents Al_2O_3 nanoparticles (d = 13 nm) and 2-2-2-methoxyethoxyethoxy acetic acid were purchased from Sigma-Aldrich. Isostearic acid was purchased from Nissan Chemical Industries and was used without further purification. Toluene and isopropanol were supplied by VWR Chemicals. Plastic film (75 µm thickness), composed of 5-ply ethylene vinyl acetate/ ethylene vinyl acetate/ poly-vinylidene dichloride/ ethylene vinyl acetate/ ethylene vinyl acetate was selected as the substrate in this study.

Synthesis of the carboxylate functionalized Al_2O_3 nanoparticles The isostearate and 2-2-2-methoxyethoxyethoxy acetate functionalised Al_2O_3 nanoparticles were synthesized using a similar method to what we have previously reported[4, 5]. In a typical experiment, Al_2O_3 nanoparticles (1.0 mol equiv.) were refluxed with isostearic or 2-[2-(2-methoxyethoxy)ethoxy]acetic acid (1.4 mol equiv.) in toluene for twenty-four hours. The volume of toluene was controlled such that 350 mL

was added per 15.0 g of Al_2O_3. Purification of the nanoparticles was achieved through centrifuging the reaction suspension at 5000 rpm for one hour. Following this, the supernatant was removed and the nanoparticles were suspended in isopropanol. This suspension was mixed using a spatula and then centrifuged at 5000 rpm for one hour. The supernatant from this suspension was then discarded. This procedure was repeated two further times using isopropanol, and then once using ethanol. When this had been completed the nanoparticle slurries were dried at 100 °C for at least four hours.

Preparation of the spray coating suspensions Isopropanolic suspensions containing 2 %wt Al_2O_3 nanoparticles were prepared that contained different amounts of isostearate and 2-[2-(2-methoxyethoxy)ethoxy] acetate functionalised Al_2O_3 nanoparticles. Despite varying the relative amounts of these two particles in the suspensions the total concentration of the particles was maintained at 2 %wt. Samples were prepared containing 0, 10, 20, 30, 40, 50, 60, 70, 80, 90, and 100% isostearate functionalised Al_2O_3 nanoparticles. 2-[2-(2-methoxyethoxy)ethoxy] acetate functionalised Al_2O_3 nanoparticles made up the balance for each suspension. These suspensions were used to embed particles into the plastic during the thermal embedding experiments.

Thermal embedding of the nanoparticles into the plastic film Plastic film was first attached to the back of a glass petri dish. The film was then heated on a hot plate until it had reached its melting temperature (80-90 °C), whereupon the material was observed to plastically deform. Following this, functionalised Al_2O_3 nanoparticles were sprayed onto the heated plastic from the 2 %wt isopropanolic suspensions using a hand-held spray gun. Five layers of nanoparticles were sprayed onto the plastic before the samples were sonicated in isopropanol. Samples were continually heated throughout the entire number of passes of spray coating. Following each pass of spray coating, pressure was exerted onto the coated plastic through rolling a glass rod across the surface of the samples using the middle and index fingers. The pressure was controlled so that the rolling action

did not damage the substrate. The pressure was not measured during the process, although it has been observed that middle and index fingers typically exert forces ranging between 35-50 N[26]. This was carried out when isopropanol was no longer observed on the surfaces and was carried out in order to promote embedding of the nanoparticles into the plastic. Once the spray coating had been completed, samples were sonicated in isopropanol for ten minutes in order to remove loose particles that had not been embedded into the plastic, and then dried using a gentle stream of nitrogen.

Characterisation Apparent water contact angles (CAs) were measured using a Krüss DSA25 Drop Shape Analyser and the sessile drop method. Measurements were made using 4 μL droplets of deionised water under ambient conditions. The CAs quoted in this study are the average of three measurements performed at different locations on the surfaces; uncertainties are the associated standard deviations. Advancing and receding CA measurements were made by dosing a 5.0 μL droplet with H_2O at a rate of 0.5 μLs^{-1} until its final volume reached 35.0 μL. Water was then removed from the droplet at a rate of 0.5 μLs^{-1} until its volume returned to 5.0 μL. During the sliding angle measurements samples were tilted from 0-90^o at a rate of 60$^o min^{-1}$. Atomic force microscopy (AFM) was carried out using a JPK Nanowizard AFM in tapping mode. The root-mean-squared roughness measurements that are discussed in the surface characterisation section were performed on the 5 × 5 μm^2 areas displayed in figure 1. Scanning electron microscopy (SEM) was carried out using a Hitachi S4800 scanning electron microscope equipped with a Silicon Drift X-Max EDX detector. Samples that were used to study the cross section of the coated material were prepared through mechanically cutting the coated material at positions towards the centre of samples. Typically, the sample size used during the preparation of these specimens was less than 5 cm × 5 cm. Cross-sectional imaging was performed on the newly created edges. EDX spectra were analysed using Inca EDX software (Oxford Instr.). X-ray photoelectron spectroscopy was performed using an

Axis Supra XPS using a monochromated Al K_α source and large area slot mode detector (ca. 300 × 800 μm^2) analysis area. Spectra were recorded using a charge neutralizer to limit differential charging and binding energies were calibrated to the main hydrocarbon peak (BE 284.8 eV). XPS spectra were analysed using CASA software. Scratch testing was carried out in accordance to ISO 1518-1:2019. During testing, a 1 mm tungsten carbide tip was moved laterally across the substrates over a distance of 10 cm. The load was kept constant during sliding. Different weights (2, 5, 10, 20 and 50 g) were used during the tests to investigate the durability of the nanoparticle films. Anti-fogging experiments were performed through attaching samples to a lid of a sealed box that contained a vessel of boiling water. Samples were kept within the box for ten minutes to allow water vapour to condense onto the surface of the samples. SEM, AFM, and XPS were carried out on the as received plastic substrate, and the heated and non-heated isostearate functionalised nanoparticle films, before and after sonication in isopropanol. CA measurements were carried out on these surfaces and also plastic that had been embedded with both isostearate and the 2-[2-(2-methoxyethoxy)ethoxy]acetate functionalised nanoparticles. The durability tests were performed on films formed from the isostearate functionalised nanoparticles that had been deposited onto the non-heated plastic, and the plastic following thermal embedding of the isostearate functionalised nanoparticles.

3. Results and discussion

Surface characterization

SEM, AFM and XPS were used to study the surface morphology and elemental composition of the heated plastic following thermal embedding of the isostearate functionalised Al_2O_3 nanoparticles. SEM of the plastic after spray coating showed that large amounts of non-embedded nanoparticles

were deposited onto the material during spraying (Fig. S1, see ESI). Removal of non-embedded nanoparticles was readily achieved through sonication of the heat-treated substrates in isopropanol. Following sonication, SEM revealed that agglomerates of nanoparticles had become embedded within the surface of the plastic (Fig. 1c). By comparison, the morphology of sonicated specimens that had not been heated was similar to that of the uncoated plastic (Fig. 1a and Fig. S2a, see ESI). This indicates that the particles do not become embedded into the plastic when the spray coating is performed under ambient conditions. Visually, it was also possible to gain an understanding of the success of the embedding experiments from the appearance of the samples. Samples embedded with the nanoparticles remained white after sonication, unlike the non-heated specimens (Fig. S3, see ESI).

AFM showed that the topography of the plastic that had been embedded with the nanoparticles was substantially rougher than the as received plastic (Fig. 1d and b). The root-mean squared roughness of the plastic after nanoparticle embedding was observed to be 43.92 nm, whereas the uncoated plastic displayed a root-mean squared roughness of 13.86 nm. Residual nanoparticles were also observed on the surface of the non-heated plastic after sonication (Fig. S2b), indicating that the treatment was not completely effective at removing non-embedded particles from the substrate.

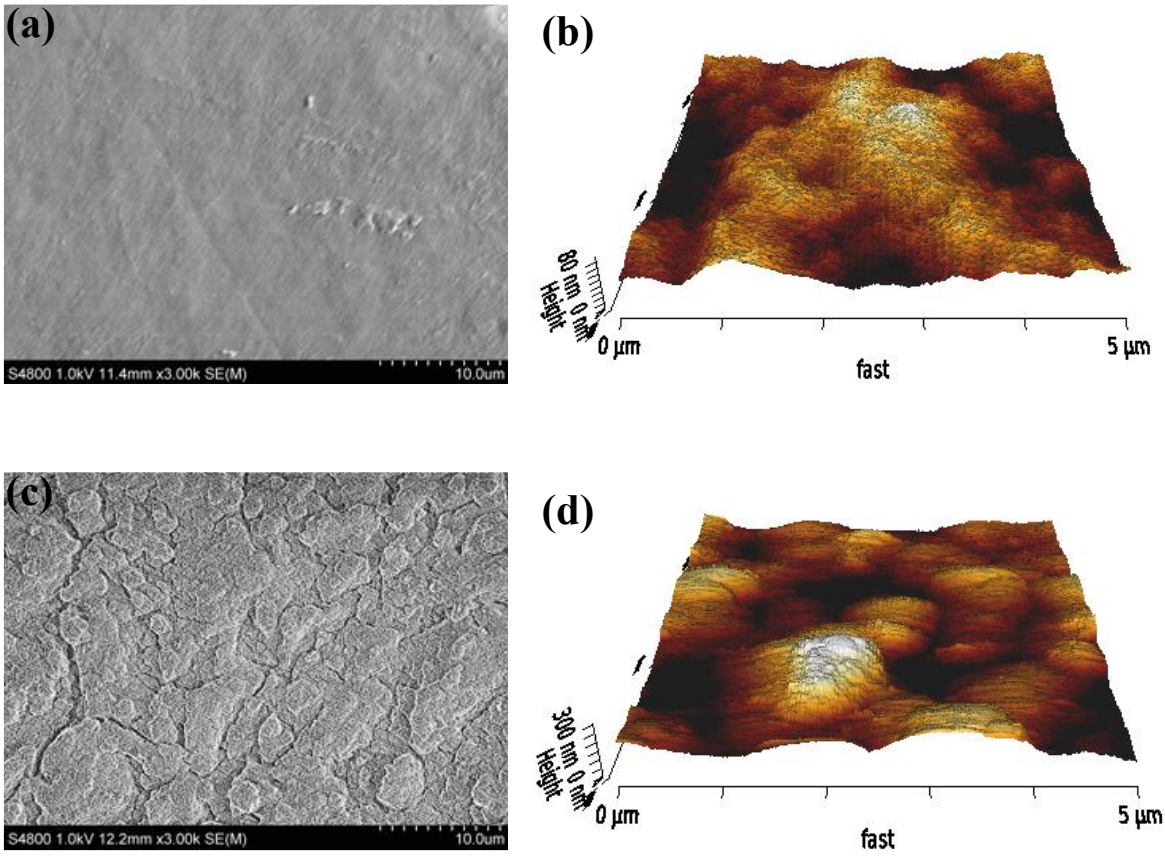

Fig 1. SEM and AFM images of the as received plastic (a) and (b), and the isostearate functionalised Al_2O_3 nanoparticles embedded into the plastic film (c) and (d).

XPS analysis was carried out on the uncoated plastic and photoelectron peaks ascribed to C, O, and N were observed in the spectrum, as shown in Fig. 2a.[27] In addition, a low intensity Al photoelectron peak was also observed. This could be attributed to the presence of residual methylaluminoxane, which is used as a co-catalyst in the olefin polymerisation process[28], however, the atomic percentage of Al was only observed to be 0.6 %, indicating that a relatively small amount of this compound was present in the surface layers. Larger amounts of Al were detected on plastic films that were spray coated with the functionalised nanoparticles and then sonicated in isopropanol (Table 1). For the heat-treated film this is ascribed to the embedded nanoparticles, whereas for the

non-heated film it is ascribed to the residual particles that were observed using AFM. XPS survey spectra of these surfaces are displayed in Fig. 2b and c.

The atomic percentage of Al observed in the heat-treated film was substantially larger than what was detected on the non-heated film (Table 1). This indicates that many more particles were present within the uppermost surface layers (0-10 nm)[29] of the plastic, confirming that the morphological changes observed using AFM and SEM were due to the thermal embedding of the nanoparticles. Analysis of the atomic percentages of O and Al showed that the Al:O ratio for the heat-treated film was approximately 1.0:1.6 (Table 1). This is similar to 1.0:1.5, the stoichiometric ratio of Al:O in Al_2O_3, which shows that the O that is detected is largely credited to the nanoparticles and not the substrate. This suggests that the embedded nanoparticles form at least the majority of the surface. By comparison, the Al:O ratio observed in the non-heated film was about 1.0:2.7, indicating that far more of the O detected is from the ethylene vinyl acetate. This is in line with the SEM data, which shows that the residual particles do not completely cover the surface of the plastic (SI Fig. S2a).

Further SEM was performed to investigate how deep the nanoparticles became embedded into the plastic during heating. Based on the magnification and EDX maps for Al and O (Figure 3 (d) and (e) respectively), it can be observed that some of the nanoparticles penetrate into the bulk of the material. This indicates that the particles embed deeper into the plastic than the depth that is sampled using XPS (0-10 nm)[29].However, the data also show that substantially more particles remain embedded in the surface of the plastic rather than penetrating into the bulk of the plastic. The Al that is detected on the non-coated side of the material could potentially arise from the transfer of nanoparticles from the coated to non-coated side when the specimen was cut to prepare the cross section. Given that the diameter of the Al_2O_3 nanoparticles used in this study was 13 nm, this data

225 suggests that the depth of thermal embedding of the particles into the plastic is of the order of
226 hundreds of times the particle diameter.

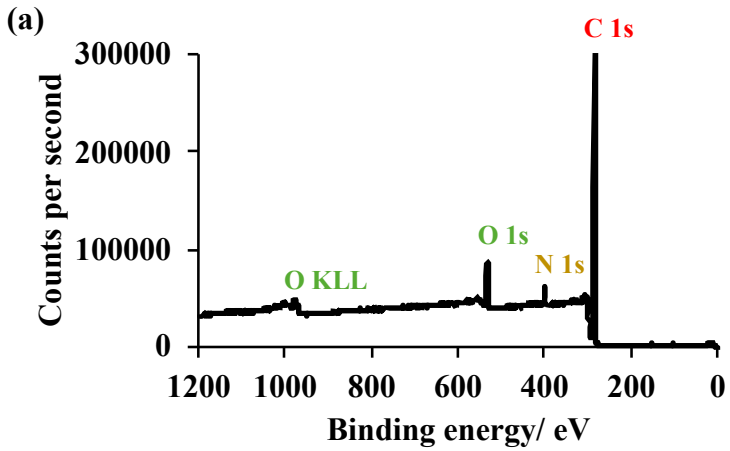

227

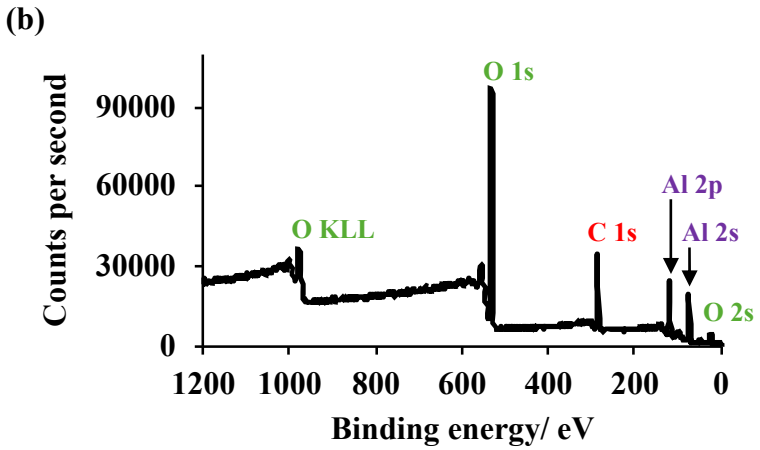

228

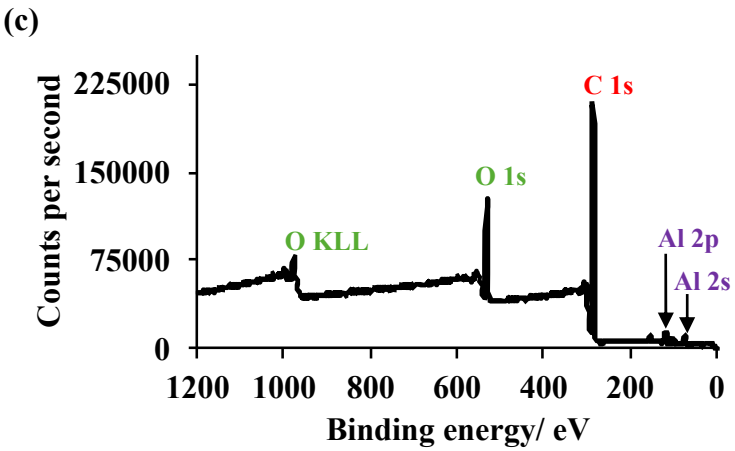

Fig 2. XPS survey spectra of the as received plastic (a), and isostearate functionalised Al_2O_3 nanoparticles deposited onto (b) the heat-treated plastic and (c) the non-heated plastic. Spectra of the coated plastic were recorded after the surfaces had been sonicated in isopropanol.

Table 1. Atomic percentages of elements that were observed on the as received plastic, plastic after (1) spray coating with the isostearate functionalised nanoparticles and (2) sonication in isopropanol, and plastic embedded with the isostearate functionalised nanoparticles. Small amounts of Si were also observed on these surfaces which complete the balances. This is ascribed to compounds found on the surface of laboratory gloves[30].

Element	Plastic	Non-heated film	Heat-treated film
C	88.1 ± 0.8	76.7 ± 5.2	33.2 ± 1.9
O	8.0 ± 0.6	15.3 ± 2.9	40.9 ± 1.3
N	2.8 ± 0.4	Not detected	Not detected
Al	0.6 ± 0.5	5.7 ± 1.9	26.0 ± 0.7

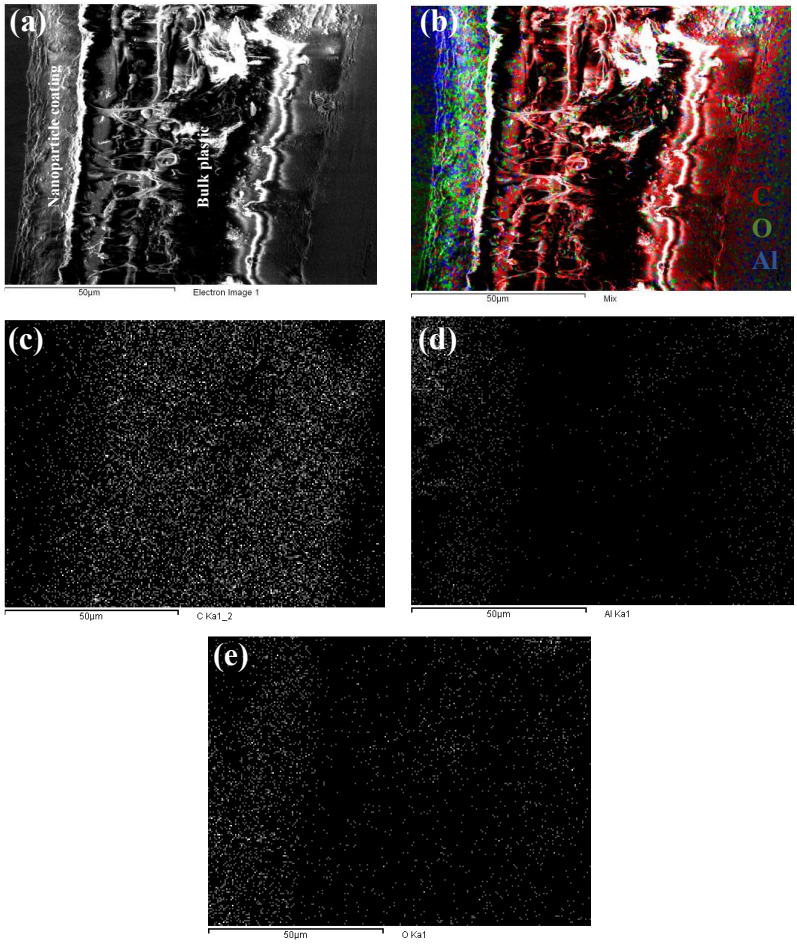

239

240 **Fig 3**. 5.0 kV SEM image (a) and EDX map (b) of the cross section of the plastic substrate
241 embedded with the isostearate functionalised nanoparticles. EDX maps of the individual elements
242 C, Al, and O, are shown in (c), (d), and (e) respectively. The orientation of the sample in the images
243 is such that the surface embedded with the particles is perpendicular to the scale bars of the images.
244 EDX spectra were acquired using a 5.0 kV accelerating voltage.

245

246

247

Wetting behaviour

The CA of the as received plastic was observed to be approximately 88 ± 2°. Thermally embedding the isostearate functionalised nanoparticles into the plastic was observed to make it substantially more hydrophobic and display a CA of about 152 ± 3°. This behaviour is due to both low surface energy, which is ascribed to the chemical functionality found on the surface of the particles, and roughness that is created when the particles become embedded into the plastic[31]. Embedding 2-[2-(2-methoxyethoxy)ethoxy] acetate functionalised Al_2O_3 nanoparticles into plastic was also investigated in order to further study the scope of this methodology. It was observed that the CA of the plastic embedded with these nanoparticles was about 37.2 ± 7.2°, which is ascribed to the hydrophilicity of the ether functional groups of the carboxylate chains. Interestingly, this coating was not superhydrophilic as observed in our previous publication[5]. This indicates that the plastic surrounding the nanoparticles also has a bearing on the wettability of the surface.

Dynamic contact angle measurements were employed to probe the surface heterogeneity[32, 33] of plastic samples embedded with the isostearate-functionalised nanoparticles. It was observed that the receding CA of plastic embedded with the nanoparticles was substantially lower than when the particles were spray-coated onto the material under ambient conditions (Table 2). As a consequence of this, plastic embedded with the particles showed a much larger contact angle hysteresis, relative to the non-heated nanoparticle film. In line with the high contact angle hysteresis, nanoparticle embedded plastic also showed a larger sliding angle compared to the non-heated nanoparticle film (Table 2). This indicates that plastic embedded with nanoparticles shows less effective self-cleaning behaviour relative to nanoparticle films spray-coated onto the plastic at ambient conditions.

Surfaces where water droplets adhere strongly and show CAs greater than 150° are often observed in nature[34, 35]. Petals are examples of such surfaces[34]. In these systems it has been postulated that the high adhesive force that droplets experience on these surfaces is due liquid penetrating into larger grooves that are formed between microstructures, and is thus indicative of surface heterogeneity[34]. Consideration of the dynamic wetting and sliding angle data for the embedded nanoparticle film suggests that this surface exhibits petal-like wetting behaviour where the high adhesion is caused by water penetrating into grooves formed between the microstructures[34]. AFM imaging showed that the embedded nanoparticles displayed a root mean squared roughness similar to when the particles are deposited onto the plastic at room temperature[36] (222 nm versus 210 nm), which suggests that topographic variations that could affect this behaviour do not exist on the nanoscale. The AFM image of the embedded particles from which this measurement was performed is displayed in Fig. S4. This is compared to our previously published data relating to nanoparticle films deposited onto the same plastic substrate (Table 1 and Fig. S6 (b) in reference 36).

Table 2. Dynamic CAs and tilt angles of the as received plastic, and the plastic after deposition of isostearate functionalised Al_2O_3 nanoparticle films. Values of the advancing and receding CAs for the as received plastic and the non-embedded particles are taken from our previous publication[36].

Surface	Advancing CA (°)	Receding CA (°)	Hysteresis (°)	Sliding angle (°)
Plastic	110 ± 1	84 ± 2	26	56 ± 17
Non-heated film	160 ± 4	147 ± 5	13	7 ± 2
Embedded film	155 ± 3	106 ± 3	49	21 ± 11

Further work was carried out to investigate whether thermally embedding different mass fractions of these nanoparticles could be used to control the wettability of the plastic. It was observed that the CA could be steadily lowered from about 150° to 115°, with reasonable control, by reducing the amount of the hydrophobic nanoparticles in the coating (Fig. 4). However, a larger drop in the CA was observed when the mass of the hydrophobic nanoparticles was reduced below forty percent. Here the CA was observed to be reduced from 115° to approximately 60-65°. This could indicate that there exists a ratio of hydrophobic to hydrophilic moieties on the nanoparticles above which it becomes substantially more favourable for water droplets to spread on the surface.

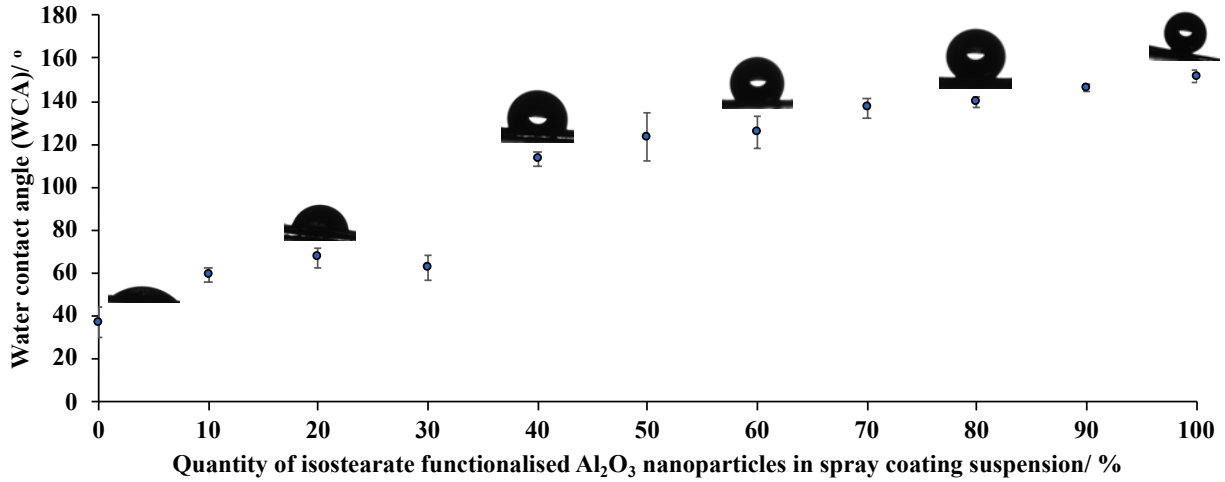

Fig 4. CAs of the plastic substrate embedded with different amounts of isostearate and 2-2-2-methoxyethoxyethoxy acetate functionalised Al_2O_3 nanoparticles. For each coating, the balance is made up by the 2-2-methoxyethoxyethoxy acetate functionalised Al_2O_3 nanoparticles.

Durability and anti-fogging behaviour

The durability of the plastic embedded with the isostearate functionalised nanoparticles was further studied to evaluate the potential utility of these coatings. In addition to being sonication

resistant, the embedded nanoparticles were observed to be resistant to finger-wiping and tape peel tests using M4 Scotch tape. CAs between 145-150° were observed after subjecting the coating to abrasion using fingers and one single tape peel test, indicating at least the majority of nanoparticles remained embedded in the plastic (Fig. S5 (a) and (b)). SEM showed that these samples possessed similar surface morphologies to the surface before the durability tests, in support of this assertion (Fig. S6 (a)-(c)). Similar durability has also been reported for silica nanoparticles embedded in poly(methyl methacrylate)[37]. However, water droplets were more adherent onto the surfaces following these treatments and would not roll off during sliding angle measurements. This could suggest that some nanomaterial was removed during the tests, despite the samples showing similar surface morphologies. The CAs of the nanoparticles embedded in the plastic was observed to be slightly reduced to about 139° after five tape peel tests (Fig. S5 (c)), indicating the loss of some nanoparticles from the substrate. This was confirmed using SEM, which showed that discrete areas of the plastic existed that appeared smoother as is shown in Fig. S6 (d).

By comparison, particles could be readily removed from isostearate functionalised nanoparticle films deposited on the non-heated plastic through finger-wiping or through sonication. This generated surfaces that displayed CAs of about 102 and 90º respectively (Fig. S7 (b) and (c)). This indicated that at least the majority of particles had been removed from the surfaces, which was confirmed using SEM (Fig. S8 (a) and (b) and Fig. S2 (a)). The non-heated films retained their superhydrophobicity after one tape peel test, but showed a CA of about 104º after five tape peel tests, indicating particle removal. This was once again confirmed by SEM (Fig. S8 (c)).

Scratch testing was also carried out to further investigate the durability of the plastic embedded with the isostearate functionalised nanoparticles. Optically visible scratches were observed right across nanoparticle films spray coated onto the non-heated plastic, for all loads greater

than 2 g (Fig. 5a). By comparison, scratches into the plastic embedded with the nanoparticles were only faintly optically visible when the substrate was subjected to higher loads (20 or 50 g) (Fig. 5b). SEM analysis showed that large amounts of nanoparticles had been removed and/ or displaced when the non-heated substrate was scratched under a 5 g load (Fig. 6a). By comparison, it was difficult to identify the wear scars on plastic specimens that had been thermally embedded with the nanoparticles, even after subjecting the surface to a 50 g load during scratch testing (Fig. 6b). This indicates that embedding the particles into the plastic greatly improves their abrasion resistance and greatly enhances the durability of nanoparticle films.

Despite the absence of surface wear observed using SEM, CAs of the scratched areas of the nanoparticle-embedded plastic varied between 135-145^{o}. Furthermore, water droplets showed greater adhesion to these areas and did not slide off the surfaces, even after tilting to 90^{o}. This data suggests that some damage to the surface was occurring, despite the apparent lack of wear observed on the surface. The CA of the surfaces was not observed to be affected by the magnitude of the applied load. For example, the CAs of areas subjected to 20 and 50 g loads were both about 139^{o} (Fig. S9 (a) and (b)).

CA measurements were also performed on areas of the non-heated nanoparticle films that were scratched using the 50 g load. These areas showed a CA of about 150^{o} but they displayed sliding angles between 11 and 66^{o}. Four microlitre water droplets were used in these experiments, which have a diameter larger than that of the tip used during the tests (~ 2 mm versus ~ 1 mm). Furthermore, loose particles were also observed on the worn areas, as observed in Fig. 6a. It is plausible that both of these factors could contribute to the high hydrophobicity observed in these areas.

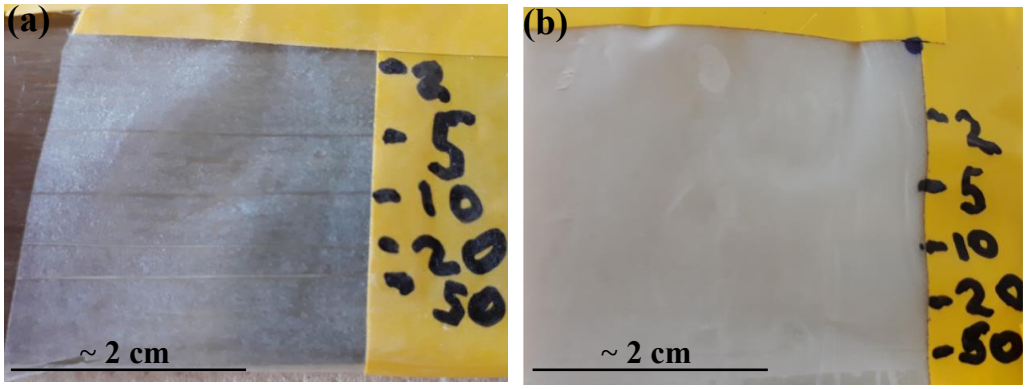

Fig 5. Images of (a) an isostearate functionalised nanoparticle film on the non-heated plastic after scratch testing, and (b) thermally embedded isostearate functionalised nanoparticles in the plastic following scratch testing. The numbers correspond to the loads in g that the surfaces were subjected to during testing.

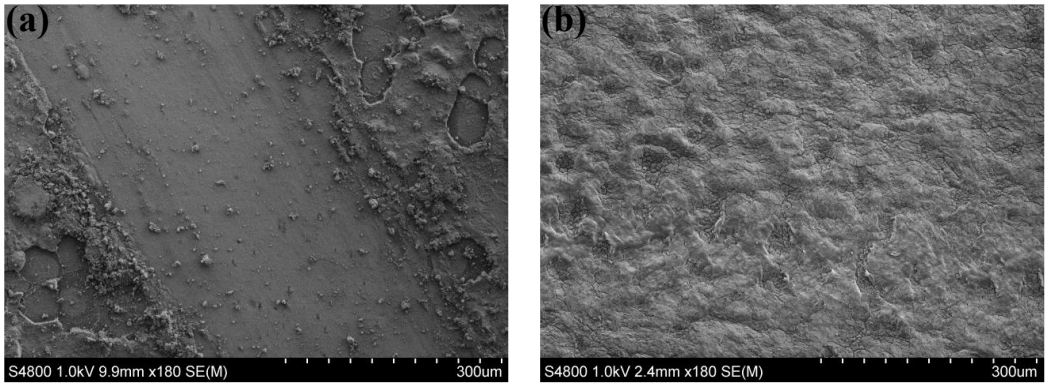

Fig 6. SEM images of (a) an isostearate functionalised nanoparticle film on the non-heated plastic after scratch testing (load = 5 g), and (b) thermally embedded isostearate functionalised nanoparticles in the plastic following scratch testing (load = 50 g).

It was also found that the embedded nanoparticle films showed anti-fogging behaviour. Fog is observed on surfaces when the diameter of water droplets exceeds half the shortest wavelength of visible light (190 nm)[38]. Visible light is scattered from droplets that are greater than this size resulting

in surfaces appearing “foggy”. Uncoated plastic, and plastic samples coated with the embedded and non-embedded isostearate functionalised nanoparticles were exposed to vapour from boiling water inside a sealed container. It was observed that water droplets of a range of different sizes were formed on the uncoated plastic (Fig. S10 (b)). By comparison, smaller water droplets were observed on the nanoparticle coated surfaces (Fig. S10 (b)), which could suggest that the larger droplets may have rolled off the surfaces during fog formation. No substantial differences between the levels of fog build-up were observed on the nanoparticle coated surfaces. This could suggest that embedding the nanoparticles into the plastic may not play a major role in affecting the potential use of this methodology to create surfaces that show fog resistance, despite the increased adhesion of water droplets onto the surface. In addition, it was also observed that the coated samples became dry substantially faster than the uncoated plastic. This could suggest that more spherical droplets show a higher evaporation rate, relative to those with lower contact angles.

4. Conclusions

In this study we report thermal embedding of nanoparticles into plastic for wettability and durability studies. Nanoparticles are functionalised with non-toxic hydrocarbons to achieve highly hydrophobic/hydrophilic surfaces. We have shown that it is possible to greatly improve the abrasion resistance of nanoparticle coatings through thermally embedding the particles into the surface of plastic. Embedding functionalized Al_2O_3 nanoparticles into the surface layers of plastic was observed to substantially improve their wear resistance, as observed through scratch and sonication tests. By comparison, coatings formed from the non-embedded nanoparticles were readily removed under these conditions. Previous work investigating improving the durability of nanoparticle coatings has involved utilising binders[7-9], or mixing the particles with commercially available adhesives[10-13]. The work reported herein advances this area of research since it shows that the

mechanical durability of nanoparticle coatings can be improved through embedding the particles into the substrate material itself, rather than through combining the particles with additives. The technique of thermal embedding of nanoparticles into plastic has never been used to control the wettability of surfaces, as well as for improving the durability of surface coatings.

Using this methodology, we have shown that surface wettability of plastic can be tailored from highly hydrophobic to highly hydrophilic depending on the chemical functionality of the nanoparticles. Embedding different mass fractions of these particles allowed this wettability control with CAs ranging from around 150 to 40°. This could mean that nanoparticle embedded plastic could be used for applications that include both waterproofing and water collection. Interestingly, plastic embedded with the hydrophobic isostearate functionalised nanoparticles was observed to show petal-like wetting behaviour[34, 35], despite showing a CA greater than 150°. As a consequence of this, our future work will investigate whether it is possible to embed particles into plastic so that it shows lotus-like wetting behaviour.

Associated content

The following file is available free of charge:

SEM image of the isostearate functionalised Al_2O_3 nanoparticles deposited onto the heated plastic before sonication in isopropanol, SEM and AFM images of the plastic substrate following (1) spray coating with the isostearate functionalised Al_2O_3 nanoparticles, and (2) sonication in isopropanol, and photograph of the as received plastic and plastic after embedding with the isostearate functionalised Al_2O_3 nanoparticles. SEM images and water CA images on plastic embedded and non-embedded with the isostearate functionalized nanoparticles after finger wiping, tape peel and mechanical test.

403 **Author information**

404 Corresponding Author

405 *E-mail: s.alexander@swansea.ac.uk

406 Notes

407 The authors declare that there are no conflicts of interest.

408

409 **Acknowledgement**

410 Financial support was provided by the Welsh Government Sêr Cymru Programme through Sêr
411 Cymru II Welsh Fellowship part funded by the European Regional Development Fund (ERDF)
412 (S.A.). We would like to acknowledge the assistance provided by Swansea University College of
413 Engineering AIM Facility, which was funded in part by the EPSRC (EP/M028267/1), the European
414 Regional Development Fund through the Welsh Government (80708) and the Sêr Solar project via
415 Welsh Government. Salts Healthcare Ltd is also acknowledged for the financial support of this
416 project (D.H).

417 **References**

418 1. X. M. Bao, J. F. Cui, H. X. Sun, W. D. Liang, Z. Q. Zhu, J. An, B. P. Yang, P. Q. La, and A. Li,
419 Facile preparation of superhydrophobic surfaces based on metal oxide nanoparticles, *Appl. Surf. Sci.*
420 303 (2014) 473–480.

421 2. N. Agrawal, S. Munjal, M. Z. Ansari, and N. Khare, Superhydrophobic palmitic acid modified
422 ZnO nanoparticles, *Ceram. Int.* 43 (2017) 14271–14276.

3. Z. T. Li, B. Lin, L. W. Jiang, E. C. Lin, J. Chen, S. J. Zhang, Y. W. Tang, F. A. He, and D. H. Li, Effective preparation of magnetic superhydrophobic Fe_3O_4/PU sponge for oil-water separation, *Appl. Surf. Sci.* 427 (2018) 56–64.

4. S. Alexander, J. Eastoe, A. M. Lord, F. Guittard, and A. R. Barron, Branched Hydrocarbon Low Surface Energy Materials for Superhydrophobic Nanoparticle Derived Surfaces, *ACS Appl. Mater. Interfaces* 8 (2016) 660-666.

5. W. A. Shatty, A. M. Lord, S. Alexander, and A. R. Barron, Tunable Surface Properties of Aluminum Oxide Nanoparticles from Highly Hydrophobic to Highly Hydrophilic, *ACS Omega* 2 (2017), 2507-2514.

6. D. Hill, H. Attia, A. R. Barron, and S. Alexander, Size and morphology dependent surface wetting based on hydrocarbon functionalized nanoparticles, *J. Colloid Interface Sci.* 543 (2019) 328-334.

7. I. S. Bayer, A. J. Davis, and A. Biswas, Robust superhydrophobic surfaces from small diffusion flame treatment of hydrophobic polymers. *RSC Adv.* 4 (2014), 264-268.

8. I. S. Bayer, K. G. Krishnan, R. Robison, E. Loth, D. H. Berry, T. E. Farrell, and J. D. Crouch, Thermal Alternating Polymer Nanocomposite (TAPNC) Coating Designed to Prevent Aerodynamic Insect Fouling, *Sci. Rep.* 6 (2016) 38459-38472.

9. M. Manca, A. Cannavale, L. De Marco, A. S. Arico, R. Cingolani, and G. Gigli, Durable Superhydrophobic and Antireflective Surfaces by Trimethylsilanized Silica Nanoparticles-Based Sol-Gel Processing, *Langmuir* 25 (2009) 6357-6362.

10. B. Chen, J. Qiu, E. Sakai, N. Kanazawa, R. Liang, and H. Feng, Robust and Superhydrophobic Surface Modification by a “Paint + Adhesive” Method: Applications in Self-Cleaning after Oil Contamination and Oil−Water Separation, *ACS Appl. Mater. Interfaces* 8 (2016), 17659-17667.

445 11. Y. Si, F. Yang, and Z. Guo, Bio-inspired one-pot route to prepare robust and repairable micro-
446 nanoscale superhydrophobic coatings, *J. Colloid Interface Sci.* 498 (2017) 182-193.

447 12. Y. Lu, S. Sathasivam, J. Song, C. R. Crick, C. J. Carmalt, and I. P. Parkin, Robust self-cleaning
448 surfaces that function when exposed to either air or oil, *Science* 347 (2015), 1132-1135.

449 13. D. Ebert, and B. Bhushan, Transparent, Superhydrophobic, and Wear-Resistant Coatings on
450 Glass and Polymer Substrates Using SiO_2, ZnO, and ITO Nanoparticles, *Langmuir* 28 (2012) 11391-
451 11399.

452 14. D. Lithner, Å. Larsson, and G. Dave, Environmental and health hazard ranking and assessment
453 of plastic polymers based on chemical composition, *Sci. Total Environ.* 409 (2011), 3309-3324.

454 15. T. Karakouz, B. M. Maoz, G. Lando, A. Vaskevich, and I. Rubinstein, Stabilization of Gold
455 Nanoparticle Films on Glass by Thermal Embedding, *ACS Appl. Mater. Interfaces*, 3 (2011), 978-
456 987.

457 16. Q. Xi, X. Chen, D. G. Evans, and W. Yang, Gold Nanoparticle-Embedded Porous Graphene
458 Thin Films Fabricated via Layer-by-Layer Self-Assembly and Subsequent Thermal Annealing for
459 Electrochemical Sensing. *Langmuir* 28 (2012) 9885-9892.

460 17. J. Prakash, J. C. Pivin, and H. C. Swart, Noble metal nanoparticles embedding into polymeric
461 materials: From fundamentals to applications. *Adv. Colloid Interface Sci.* 226 (2015) 187-202.

462 18. V. Zaporojtchenko, T. Strunskus, J. Erichsen, and F. Faupel, Embedding of noble metal
463 nanoclusters into polymers as a potential probe of the surface glass transition, *Macromolecules* 34
464 (2001) 1125-1127.

465 19. J. H. Teichroeb, and J. A. Forrest, Direct Imaging of Nanoparticle Embedding to Probe
466 Viscoelasticity of Polymer Surfaces, *Phys. Rev. Lett.* 91 (2003) 016104.

20. A. L. Stepanov, Synthesis of Silver Nanoparticles in Dielectric Matrix by Ion Implantation: A Review. *Rev. Adv. Mater. Sci.* 26 (2010) 1-29.

21. D. K. Avasthi, Y. K. Mishra, D. Kabiraj, N. P. Lalla, and J. C. Pivin, Synthesis of metal–polymer nanocomposite for optical applications. *Nanotechnology*, 18 (2007) 125604-125608.

22. Sharp, J. S.; Teichroeb, J. H.; Forrest, J. A. The properties of free polymer surfaces and their influence on the glass transition temperature of thin polystyrene films. *Eur. Phys. J. E: Soft Matter Biol. Phys.*, **2004**, *15*, 473-487.

23. Weber, R.; Grotkopp, I.; Stettner, J.; Tolan, M.; Press, W. Embedding of Gold Nanoclusters on Polystyrene Surfaces: Influence of the Surface Modification on the Glass Transition. *Macromolecules*, **2003**, *36*, 9100-9106.

24. S. Prakash, T. Chakrabarty, A. K. Singh, and V. K. Shahi, Polymer thin films embedded with metal nanoparticles for electrochemical biosensors applications. *Biosens. Bioelectron.* 41 (2013) 43-53.

25. C. Hanisch, A. Kulkarni, V. Zaporojtchenko, and F. Faupel, Polymer-metal nanocomposites with 2- dimensional Au nanoparticle arrays for sensoric applications. *J. Phys.: Conf. Ser.* 100 (2008) 052043.

26. K. J., Bretz, Á. Jobbágy, and K. Bretz, Force measurement of hand and fingers. *Biomechanica Hungarica* 3.1 (2010).

27. J. F. Moulder, W. F. Stickle, P. E. Sobol, and K. D. Bomben in Handbook of X-ray Photoelectron Spectroscopy, *Perkin-Elmer Corporation* 1992, Appendix H, pp. 256.

28. D. W. Sauter, M. Taoufik, and C. Boisson, Polyolefins, a Success Story, *Polymers* 9 (2017) 185-198.

29. M. P. Seah and W. A. Dench, Quantitative electron spectroscopy of surfaces: A standard database for electron inelastic mean free paths in solids. *Surf. Interface Anal.* 1 (1979), 2-11.

30. A. Plasencia, J. D. Piasecki, and B. R. Strohmeier, XPS Surface Characterization of Disposable Laboratory Gloves and the Transfer of Glove Components to Other Surfaces, *Spectroscopy* 27 (2012) 36-47.

31. M. Miwa, A. Nakajima, A. Fujishima, K. Hashimoto, and T. Watanabe, Effects of the Surface Roughness on Sliding Angles of Water Droplets on Superhydrophobic Surfaces, *Langmuir*, 16 (2000) 5754-5760.

32. J. Drelich, and J. D. Miller, The Effect of Solid Surface Heterogeneity and Roughness on the Contact Angle/Drop (Bubble) Size Relationship, *J. Colloid Interf. Sci.* 164 (1994) 252–259.

33. J. Drelich, J. D. Miller, and R. J. Good, The Effect of Drop (Bubble) Size on Advancing and Receding Contact Angles for Heterogeneous and Rough Solid Surfaces as Observed with Sessile-Drop and Captive-Bubble Techniques, *J. Colloid Interf. Sci*. 179 (1996) 37-50.

34. L. Feng, Y. Zhang, J. Xi, Y. Zhu, N. Wang, F. Xia, and L. Jiang, Petal effect: a superhydrophobic state with high adhesive force, *Langmuir* 24 (2008) 4114-4119.

35. Z. Cheng, M. Du, H. Lai, N. Zhangab, and Kening Sun, From petal effect to lotus effect: a facile solution immersion process for the fabrication of super-hydrophobic surfaces with controlled adhesion, *Nanoscale* 5 (2013) 2776-2783.

36. D. Hill, Andrew R. Barron, and S. Alexander, Comparison of hydrophobicity and durability of functionalized aluminium oxide nanoparticle coatings with magnetite nanoparticles–links between morphology and wettability, *J. Colloid Interf. Sci.* 555 (2019) 323-330.

510 37. N. Mizoshita and H. Tanaka, Versatile Antireflection Coating for Plastics: Partial Embedding of
511 Mesoporous Silica Nanoparticles onto Substrate Surface, *ACS Appl. Mater. Interfaces* 8 (2016)
512 31330-31338.

513 38. Z. Sun, T. Liao, K. Liu, L. Jiang, J. H. Kim, and S. X. Dou, Fly-Eye Inspired Superhydrophobic,
514 Anti-Fogging Inorganic Nanostructures, *Small* 10 (2014) 3001-3006.

515

516

517

518

519

520 TOC

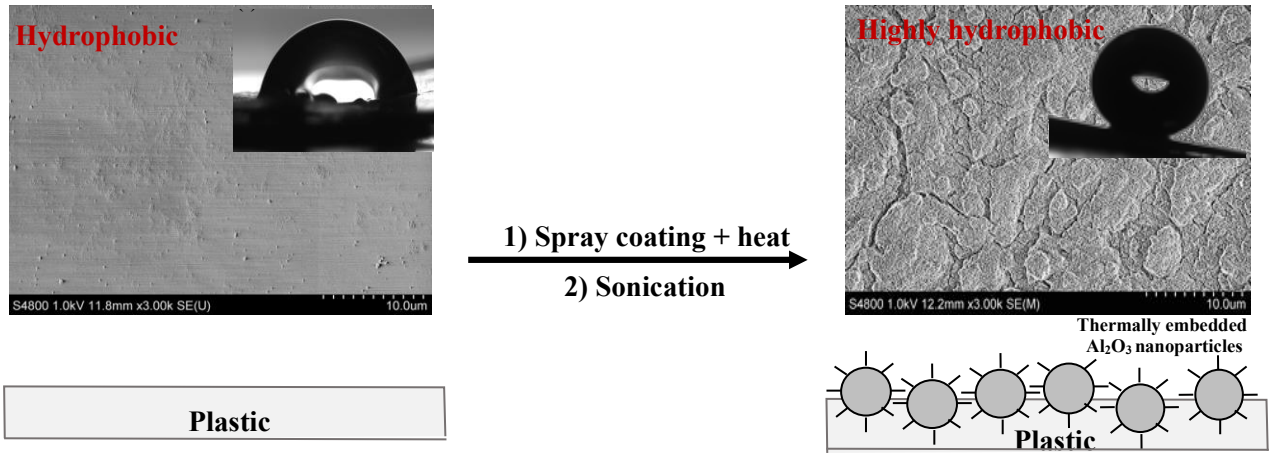

521